



Cite this: *Soft Matter*, 2023, 19, 1617

Received 22nd September 2022,
Accepted 31st January 2023

DOI: 10.1039/d2sm01284g

rsc.li/soft-matter-journal

Reprogrammable allosteric metamaterials from disordered networks†

Nidhi Pashine,^{id} Amir Mohammadi Nasab^{id} and Rebecca Kramer-Bottiglio^{id}*

Prior works on disordered mechanical metamaterial networks—consisting of fixed nodes connected by discrete bonds—have shown that auxetic and allosteric responses can be achieved by pruning a specific set of the bonds from an originally random network. However, bond pruning is irreversible and yields a single bulk response. Using material stiffness as a tunable design parameter, we create metamaterial networks where allosteric responses are achieved without bond removal. Such systems are experimentally realized through variable stiffness bonds that can strengthen and weaken on-demand. In a disordered mechanical network with variable stiffness bonds, different subsets of bonds can be strategically softened to achieve different bulk responses, enabling a multiplicity of reprogrammable input/output allosteric responses.

1 Introduction

Mechanical metamaterials are materials with unusual mechanical properties not commonly seen in nature, which arise predominantly due to clever structural design rather than material composition. There has been considerable interest in metamaterials that show novel material responses, including metamaterials that can exhibit more than one mechanical response.^{1–6}

In recent years, there has been notable development of metamaterials made from disordered systems. In a system composed of a disordered network of nodes connected by bonds, each bond contributes differently to the bulk properties of the system.⁷ This variation can be utilized by modifying individual bonds in a way that the system evolves to have a specific, programmed response. One example is a disordered mechanical network wherein an output strain between two nodes is tuned in response to an input strain applied between two source nodes, where both sets of nodes are located along the periphery of the network.⁸ A mechanical network with a long-range interaction between input and output sites is called an “allosteric” metamaterial, as allostery is the process by which biological macromolecules transmit the effect of binding at one site to another (often distal) site.

Allosteric responses have been designed in disordered mechanical networks in various ways such as bond pruning,^{8,9} network evolution,^{10,11} as well as by using local design rules.^{12,13} In the case of bond pruning (*i.e.*, the complete removal of network bonds),

once a programmed behavior is designed into a system, the output response is immutable.^{7,8,13,14} To enable tunable and recoverable allosteric metamaterial responses, we seek approaches to vary the stiffness of select bonds on-demand. With variable stiffness bonds, a subset of bonds could be softened to achieve one target response, and another set softened to achieve a completely different output response. This approach removes the need to prune bonds and enables any new target response to be achieved while all prior responses remain fully recoverable.

The field of soft robotics has recently seen substantial development of novel composite materials with tunable material properties, especially material stiffness. A variety of methods have been employed to attain variable stiffness,¹⁵ including pneumatic jamming,^{16,17} magnetorheological and electrorheological materials,^{18–21} shape memory polymers and alloys,^{22–25} liquid crystal elastomers,^{26–28} and phase-changing materials.^{29–33} Typically derived from metallic alloys, waxes, or thermoplastic polymers, encapsulated phase-changing materials exhibit a decrease in modulus *via* the transition from solid to liquid, and raise in modulus *via* the reverse (solidification) transition. One phase-changing material gaining traction in the literature is Field’s metal, a eutectic alloy of bismuth, indium, and tin known for its low melting point of $T_m = 62$ °C and non-hazardous composition.^{34–41}

Our instantiation of a re-programmable allosteric metamaterial is realized through a disordered mechanical network wherein we replace a predetermined set of inert bonds with variable stiffness bonds, which are fabricated by incorporating Field’s metal cores in soft silicone shells. A variable stiffness bond is in the high-stiffness state when the Field’s metal core is solid and in the low-stiffness state when the core is liquefied using an embedded copper heater. The bond network is designed by incorporating local stiffness as a parameter in

School of Engineering & Applied Science, Yale University, New Haven, CT, 06520, USA. E-mail: rebecca.kramer@yale.edu

† Electronic supplementary information (ESI) available. See DOI: <https://doi.org/10.1039/d2sm01284g>

simulations and varying the bond stiffness to modify the mechanical input/output response between two peripheral node sets. When different sets of the variable stiffness bonds are softened, different allosteric responses are achieved with full reversibility and re-programmability.

2 Design algorithm

Our proposed mechanical network is a spring network inspired by Rocks *et al.* 2017.⁸ The networks are generated from random configurations of jammed soft disks in 2D.⁴² By joining the centers of the disks with an unstretched central-force spring, these random jammed packings are converted into disordered spring networks. With a network of N nodes and N_b bonds, the authors of Rocks *et al.* tuned the output strain ε_{out} between two nodes in response to the input strain ε_{in} applied between two source nodes, where both sets of nodes are located far away from each other within the same network—a so-called allosteric response. In this work, we make allosteric networks by modifying the pruning algorithm presented in ref. 13 to a tuning algorithm that is based on local stress distributions in our system.

Starting with simulations of disordered networks with periodic boundaries, we randomly choose two pairs of nodes halfway across the system to be our source and target nodes. The success of our network design is measured in terms of the ratio of strain at the target nodes to the applied input strain at the source nodes; strain ratio, $\eta = \varepsilon_{\text{out}}/\varepsilon_{\text{in}}$. In our initial network, each bond has an initial spring constant of $k_{\text{stiff}}^i = \mathcal{K}_{\text{stiff}}^0/l_i$, where $\mathcal{K}_{\text{stiff}}^0$ is a constant and l_i is the length of bond i . Our design algorithm identifies a set of bonds j in $\{B_{\text{soften}}\}$, which when softened to a spring constant of $k_{\text{soft}}^j = \mathcal{K}_{\text{soft}}^0/l_j$ create an allosteric interaction between the source and target sites. To tune an allosteric response, we choose the source and target sites, the desired strain ratio (η^{goal}), and the stiffness ratio of the bonds, $\mathcal{R} = \mathcal{K}_{\text{soft}}^0/\mathcal{K}_{\text{stiff}}^0$. Notably, the initial network contains no soft modes and any stresses from an applied strain would dissipate locally. Therefore, the initial strain ratio of these networks is $\eta^0 \approx 0$.

The set of bonds to be softened, $\{B_{\text{soften}}\}$, is determined based on the stress distribution in the network under externally applied strains. We define T_i^{source} as the tension in bond i as a result of an applied strain at the source site and T_i^{target} as the tension in bond i due to applied strain at target site. A positive value of T_i corresponds to tension and a negative value corresponds to compression of bond i .

Our design algorithm is based on the values of T_i^{source} and T_i^{target} for each bond i . These terms calculate how much stress is channeled into each bond when a strain is applied at a particular site in the system. Previous work has shown that the product of the two terms, $T_j^{\text{source}} \times T_j^{\text{target}}$, determines the relevance of each bond in linking the source to the target.¹³ The larger the value of $T_j^{\text{source}} \times T_j^{\text{target}}$, for a given bond, the more it hinders an allosteric interaction. By softening these bonds, we allow them to stretch or compress easily, hence aiding an allosteric interaction. Until this point, the design

process is symmetric with respect to the source and the target. However, we are designing an inherently asymmetric network where the input energy is provided at the source and an output strain is expected at the target. In order to break the symmetry, we change the relative weights of T_i^{source} and T_i^{target} by softening the bond with the highest $T_j^{\text{source}} \times (T_j^{\text{target}})^n$, where n is an odd integer > 1 . Higher values of n biases the algorithm towards the target by effectively lowering the energy required to create an output strain at the target site. Hence, larger values of n lead to more efficient solutions with fewer numbers of softened bonds. On the other hand, previous work has shown that as the value of n increases, the discrepancy between simulations and experiments also increases.¹³ In this work, we choose $n = 3$ as a trade-off between these two effects.

The design algorithm is summarized in Fig. 1. We measure T_i^{source} and T_i^{target} for each bond, take a product of the two terms, and soften the bond with the largest value of $T_j^{\text{source}} \times (T_j^{\text{target}})^3$. We repeat this process iteratively until η reaches its desired value or the process fails due to creation of a localized low energy mode. For simplicity, the network drawings in Fig. 1 only show the magnitude of tensions. However, the sign of each term decides the sign of η . Softening bonds where $T_j^{\text{source}} \times (T_j^{\text{target}})^3$ is positive leads to a positive η , while softening bonds where $T_j^{\text{source}} \times (T_j^{\text{target}})^3$ is negative leads to a negative η . In this work we focus on designing networks with $\eta > 0$.

The results from simulations of allosteric responses are shown in Fig. 2. Disordered networks are often characterized by the average number of bonds coming out of each node, known as the coordination number ($\langle Z \rangle$). The networks in our simulation are isostatic at an average coordination number of $\langle Z_0 \rangle = 4$. We work with three sets of networks with a system size of 70 nodes with average coordination numbers $\langle Z \rangle = 4.5$, $\langle Z \rangle = 4.8$, and $\langle Z \rangle = 5.4$. We tune each network using the design protocol described above. Note that the design process is not dependent on the strain ratio, η . We simply keep softening bonds one at a time and call the design process successful as soon as the final strain ratio goes above the desired η . As a result, the output strain of these systems is never exactly equal to the desired η but always slightly higher than it.

Fig. 2A shows the success rate as a function of the stiffness ratio for $\eta = 1$. The stiffness ratio is given as ratio of stiffness of a softened bond to the stiffness of a regular bond, such that it can take a value between 0 and 1 and a lower stiffness ratio corresponds to a higher contrast in bond stiffnesses. The success rate rapidly declines as the stiffness ratio increases, with the best results at a stiffness ratio of a few percent (0–2%). This decrease in the success rate is expected because the mechanism that incorporates an allosteric response relies on creating a low energy mode in the system which is achieved by lowering the strain energy of a particular set of bonds—ones that are softened. Increasing the stiffness ratio increases the energy stored in the soft bonds, thereby increasing the total energy of the system and lowering the success rate. An interesting feature to note here is that the closer these systems are to isostaticity ($\langle Z \rangle = 4$), the higher the success rate. We speculate that this is a result of the vibrational response of the original

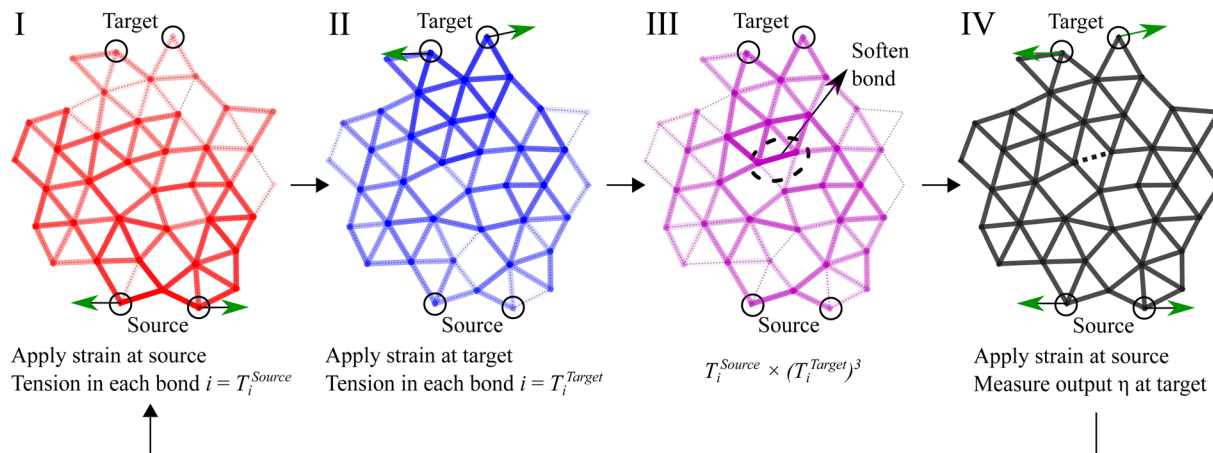


Fig. 1 A schematic of the design process. I. Apply an external strain at the source site and measure the distribution of resulting tension in the system. Darker bond corresponds to higher magnitude of tension. II. Apply an external strain at the target site and measure the resulting tension distribution. III. Using I and II, get the distribution of $T_i^{\text{Source}} \times (T_i^{\text{Target}})^3$. This identifies the bonds that are relevant to linking the source and target and creating an allosteric response. IV. Soften the selected bond (dashed line) by changing its stiffness from k_{stiff} to $k_{\text{stiff}} \times \mathcal{R}$, and measure the new η . This process is repeated iteratively till the desired η is achieved.

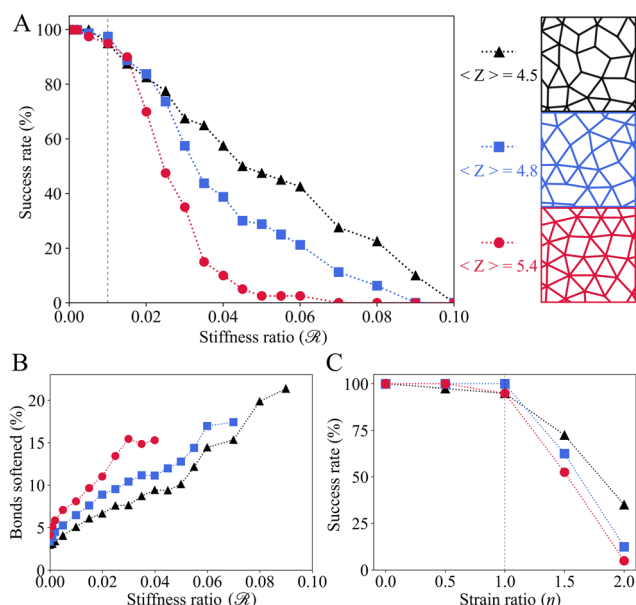


Fig. 2 (A) Success rate of networks with different coordination numbers as a function of stiffness ratio (ratio of stiffness of soft bonds to that of regular bonds). Networks were designed to have a strain ratio (ratio of strain at output nodes to the applied input strain) of 1. The vertical dashed line at 0.01 corresponds to the value of stiffness ratio used for designing networks that were built in experiments. (B) Percentage of bonds that need to be softened as a function of stiffness ratio. (C) Success rate as a function of strain ratio for a stiffness ratio of 0.01. The vertical dashed line at 1 corresponds to the strain ratio used in plots A and B.

system. It has been shown that the correlation length of vibrational modes increases as the system goes closer to isostaticity,^{43–45} and since allosteric interactions span the whole system, they are easier to achieve when extended vibrational modes are already present in the system.

Another measure of ease of designing allosteric systems is the number of bonds that need to be softened. As mentioned, our system achieves an allosteric response by lowering the energy of allosteric interaction, which is realized by softening the bonds that contribute the most to this interaction. The net change in the interaction energy depends on the number of bonds softened, as well as the amount by which their stiffness is reduced. The higher the stiffness difference between stiff and soft bonds, the fewer the number of bonds that need to be modified. This trend can be seen in Fig. 2B, where the fraction of bonds that need to be softened is plotted as a function of stiffness ratio. As expected, we see that with an increase in the stiffness ratio, more bonds need to be softened in a network. Moreover, this plot shows that the fraction of bonds that need to be softened goes up with an increase in coordination number. This finding is consistent with the data from Fig. 2A, which shows that networks with lower coordination numbers are better for designing an allosteric response.

Fig. 2C shows the success rate as a function of strain ratio, η . The success rate falls sharply as soon as η goes over 1. We note that one can achieve a more dramatic response in allosteric networks if the bonds are removed instead of softened.^{8,13} This difference is not surprising considering that softening a bond lowers the local stress in the region whereas pruning a bond gets rid of it completely. Achieving high strain ratios requires certain soft bonds to have high strains, but the residual stress in soft bonds increases rapidly with an increase in strain, thus preventing them from showing a high output response.

3 Variable stiffness bonds

Experimental realizations of allosteric networks are built out of silicone rubber sheets, with the bonds that need to be softened replaced with variable stiffness bonds. By actuating these variable bonds, we can switch between two different states of

the allosteric network. The variable bonds are made out of Field's metal and silicone, as shown in Fig. 3, and are passively stiff. By sending an electric current through co-located copper heaters, the Field's metal inside the variable bonds can be melted *via* Joule heating, resulting in a soft bond. In the stiff state, the stiffness of variable bonds is comparable to the regular silicone–rubber bonds but in their soft state, the variable bonds are orders of magnitude softer than regular bonds. Details about the construction of variable bonds, regular bonds, and experimental networks containing the bonds are included in ESI† S1.

We estimate the spring constant of the bonds by measuring the force response of both regular and variable bonds using a materials tester (Instron 3365). The response of regular as well as variable bonds in both stiff and soft states is shown in Fig. 4A. The same data is zoomed in at small strains (Fig. 4B), and low forces (Fig. 4C). The response is averaged over 5 measurements of 3 different bonds of each kind. To calculate the spring constant of each type of bond, we fit a slope to the force-displacement curve in the small strain region where the response is mostly linear. In our experiments, the stiff bonds as well as the regular bonds (apart from the ones right at the input site) experience negligible strain. On the other hand, when the variable bonds are in their soft state, they get strained to around 5%. For the present calculations, we include strains between 0 and 1.5% and get the following spring constants for each bond type: $k_{\text{regular}} = 4.1 \pm 0.2 \text{ N mm}^{-1}$, $k_{\text{stiff}} = 2.2 \pm 0.6 \text{ N mm}^{-1}$, $k_{\text{soft}} = 0.036 \pm 0.004 \text{ N mm}^{-1}$. As expected, the spring constant of bonds in the soft state is much lower than the other two. Soft bonds are 0.9% as stiff as the regular bonds, and as shown in the previous section, designing allosteric responses is very successful at this low stiffness ratio.

We note here that the bonds have a non-linear response over large strain ranges, as shown in Fig. 4. In particular, the variable bond in the stiff state gets substantially softer at larger strains. However, the stiff bonds usually do not experience large strains and therefore this non-linearity does not have a

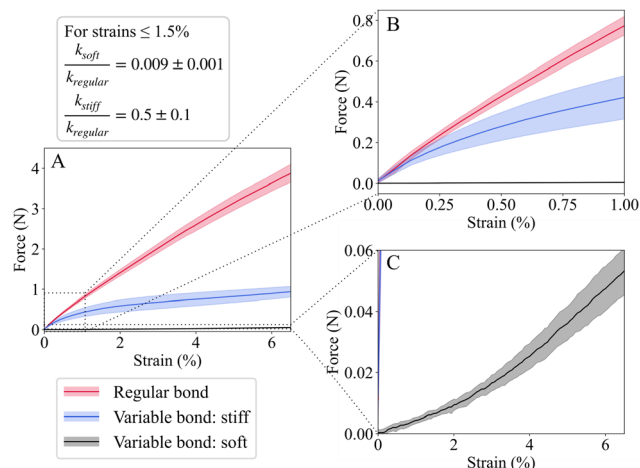


Fig. 4 (A) Force response of regular bonds (red), variable bonds in the stiff state (blue), and variable bonds in the soft state (black). Response at (B) low strains, and (C) small forces. Stiffness values (k_{soft} , k_{stiff} , k_{regular}) are obtained from the slopes of the force curves for strains between 0 and 1.5%.

significant impact on the response of our networks. The strain distribution within a simulated network is shown in ESI† S2.

4 Allosteric networks in experiments

To test the efficacy of our experimental networks, we measure their response with the variable bonds in stiff and soft states. A linear spring model is an oversimplification of real material networks, and previous studies have shown that materials have other interactions such as angle bending forces and nonlinear stress–strain response present in them.¹⁴ Therefore, only a fraction of allosteric networks designed in simulations show a comparable response in experiments.¹³

To evaluate the behavior of incorporating variable stiffness composites in a way that is decoupled from other effects in our system, we make two copies of each network that we want to test. In the first copy, C1, we take the set of selected bonds, B_{soften} , and replace them with variable stiffness bonds. In the second copy, C2, we prune the set of bonds, B_{softened} . Then we compare the response, $\eta(\text{C1})$ to $\eta(\text{C2})$. We test 3 such networks and find that $\eta(\text{C1}) = 90 \pm 5\%$ of $\eta(\text{C2})$. Since there are multiple mechanisms that lead to a loss in output response, the output response in experiments often ends up being substantially smaller than the designed response.

The designed allosteric networks show an output strain only when the correct set of variable bonds is softened. We can build multiple input and output responses in a single network and our design process guarantees that each incorporated response works independently when the corresponding set of variable bonds is softened. However, as long as different responses have allosteric pathways that do not overlap spatially, we often see that multiple allosteric responses can coexist in experiments. One such example is shown in Fig. 5(A): bonds in blue correspond to output 1, and bonds in green correspond to output 2. When the blue bonds are softened and the green bonds are

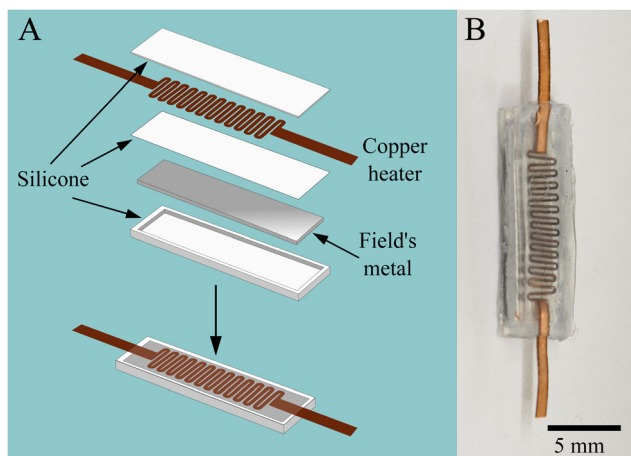


Fig. 3 (A) Schematic of a variable stiffness bond comprising of a Field's metal core and a copper heater that are sandwiched between three layers of silicone. (B) Image of a variable bond.

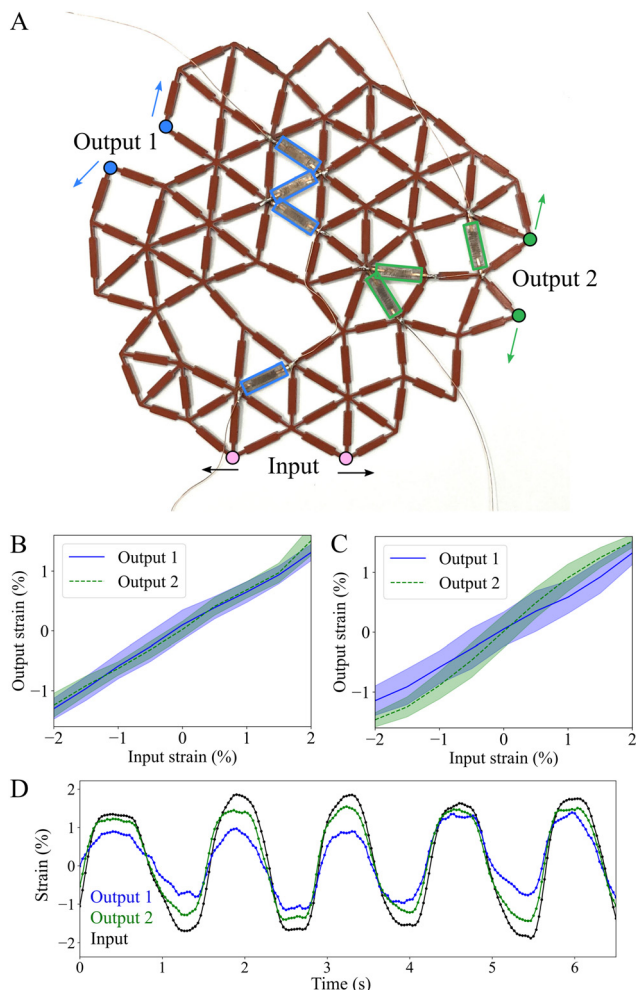


Fig. 5 (A) Allosteric network with multiple responses. Variable stiffness bonds are highlighted in blue and green. Softening blue bonds creates a response at output 1, softening green bonds shows a response at output 2, and softening both sets of bonds shows responses at output sites 1 and 2. Responses can be seen in Movie S3 (ESI†). (B) Strain at output site as a function of input strain when each response is activated individually. Output 1 is blue (solid) line and output 2 is green (dashed) line. (C) Output responses when both outputs are activated simultaneously. (D) Strain response as a function of time with both outputs activated. Cyclic input strain (black) results in output strains at output 1 (blue) and output 2 (green). Data has been smoothed, using a Savitzky–Golay filter with a window length of 300 ms, for clarity.

stiff, an applied strain at the input site results in a strain at output 1 but not at output 2. Similarly, softening just the green bonds results in a strain at output 2 but not at output 1. Fig. 5(B) shows the measured output strain responses as a function of input strain at sites 1 and 2, when each response is activated individually. The responses are linear in the small strain regime, with output at site 1, $\eta_1 = 0.64 \pm 0.01$, and output at site 2, $\eta_2 = 0.65 \pm 0.01$. Note that both responses are smaller than the designed response of $\eta = 1$. These two sets do not have any bonds in common and the pathways are spatially separated from each other. In such cases, when both the sets of bonds are softened, we see a response at both the output sites 1 and 2

without detriment to either of the outputs. Fig. 5(C) shows the output strain responses as a function of input strain, when both the responses are activated simultaneously. The output strain responses at each of the output sites are slightly different than before, with $\eta_1 = 0.60 \pm 0.02$, and $\eta_2 = 0.81 \pm 0.01$. Fig. 5(D) shows the strains at input and output sites as a function of time, where both sets of bonds have been softened and both output sites simultaneously respond to the input strain.

Although multiple responses can be designed to work simultaneously, this is not how this particular network was designed. Our design process finds independent solutions for each output which often turn out to work concurrently. Despite some experimental losses in the designed networks, our result shows that this method of designing allosteric responses with variable stiffness materials is successful and feasible.

5 Conclusions

The ability to actively tune the behavior of a mechanical metamaterial is essential for developing the next generation of materials with increased adaptability and functionality. In this work, we have demonstrated designing and building disordered allosteric metamaterials with multiple input and output responses incorporated in them that can each be individually activated on demand. To achieve this, we designed and fabricated variable stiffness bonds whose stiffness changes by two orders of magnitude between their soft and stiff states. This work brings together the active tunability of material properties and the diversity of responses that can be achieved in disordered systems to create a new kind of allosteric metamaterial.

Our work opens further avenues in both theoretical and experimental directions. We introduced material stiffness as a design parameter in disordered networks, but eventually our variable bonds exist in one of the two possible states. Further work is needed to create metamaterial systems that truly utilize the range of material properties that can be achieved through variable stiffness composites. Such a system might be able to sustain multiple responses that are not spatially separated. Additionally, our current simulation uses a simplified linear spring model which deviates from experiments, especially when extended to large system sizes or systems with a higher number of responses. More realistic simulations would give us a platform to design and build networks that can exhibit more diverse and complex responses.

A distinct feature of our design algorithm is that we use a local rule, as opposed to a global optimization. Local design rules provide an ideal framework to build adaptable materials because the system changes its properties based on local stimuli. Our success with using a variable stiffness material inspires us to consider other materials that respond to external stimuli in different ways, such as bonds that can connect and disconnect adjacent nodes or expand or shrink in length. Using a variety of materials that respond to stimuli in different ways

will substantially expand our design space and allow us to build systems with adaptable mechanical responses.

Relatedly, there has been much recent interest in mechanical memory, computing, and supervised learning in physical systems.^{12,46–51} We believe that variable bonds, and more generally the concept of locally tunable properties in material systems,^{50–53} could be applied beyond the case of allostery in materials. For example, we envision such local stiffness control may contribute toward metamaterials with adaptable force paths, bulk moduli, and computing functions.^{54,55} This paper lays groundwork for the development of adaptable smart materials that can modify their properties based on external stimuli.

Conflicts of interest

There are no conflicts to declare.

Acknowledgements

We thank F. Arceri, T. Buckner, and S. Eristoff for helpful discussions. This material is based upon work supported by the National Science Foundation under Grant No. DMREF-2118988.

Notes and references

- 1 K. Bertoldi, V. Vitelli, J. Christensen and M. van Hecke, *Nat. Rev. Mater.*, 2017, **2**, 1–11.
- 2 A. Bossart, D. M. J. Dykstra, J. van der Laan and C. Coullais, *Proc. Natl. Acad. Sci. U. S. A.*, 2021, **118**, e2018610118.
- 3 D. Hexner, *Soft Matter*, 2021, **17**, 4407–4412.
- 4 O. R. Bilal, A. Foehr and C. Daraio, *Proc. Natl. Acad. Sci. U. S. A.*, 2017, **114**, 4603–4606.
- 5 L. Jin, R. Khajetourian, J. Mueller, A. Rafsanjani, V. Tournat, K. Bertoldi and D. M. Kochmann, *Proc. Natl. Acad. Sci. U. S. A.*, 2020, **117**, 2319–2325.
- 6 S. Kamrava, D. Mousanezhad, H. Ebrahimi, R. Ghosh and A. Vaziri, *Sci. Rep.*, 2017, **7**, 46046.
- 7 C. P. Goodrich, A. J. Liu and S. R. Nagel, *Phys. Rev. Lett.*, 2015, **114**, 225501.
- 8 J. W. Rocks, N. Pashine, I. Bischofberger, C. P. Goodrich, A. J. Liu and S. R. Nagel, *Proc. Natl. Acad. Sci. U. S. A.*, 2017, **114**, 2520–2525.
- 9 J. W. Rocks, H. Ronellenfitsch, A. J. Liu, S. R. Nagel and E. Katifori, *Proc. Natl. Acad. Sci. U. S. A.*, 2019, **116**, 2506–2511.
- 10 L. Yan, R. Ravasio, C. Brito and M. Wyart, *Proc. Natl. Acad. Sci. U. S. A.*, 2017, **114**, 2526–2531.
- 11 J. Z. Kim, Z. Lu, S. H. Strogatz and D. S. Bassett, *Nat. Phys.*, 2019, **15**, 714–720.
- 12 D. Hexner, A. J. Liu and S. R. Nagel, *Proc. Natl. Acad. Sci. U. S. A.*, 2020, **117**, 31690–31695.
- 13 N. Pashine, *Phys. Rev. Mater.*, 2021, **5**, 065607.
- 14 D. R. Reid, N. Pashine, J. M. Wozniak, H. M. Jaeger, A. J. Liu, S. R. Nagel and J. J. D. Pablo, *Proc. Natl. Acad. Sci. U. S. A.*, 2018, **115**, E1384–E1390.
- 15 L. Wang, Y. Yang, Y. Chen, C. Majidi, F. Iida, E. Askounis and Q. Pei, *Mater. Today*, 2018, **21**, 563–576.
- 16 E. Brown, N. Rodenberg, J. Amend, A. Mozeika, E. Steltz, M. R. Zakin, H. Lipson and H. M. Jaeger, *Proc. Natl. Acad. Sci. U. S. A.*, 2010, **107**, 18809–18814.
- 17 D. S. Shah, E. J. Yang, M. C. Yuen, E. C. Huang and R. Kramer-Bottiglio, *Adv. Funct. Mater.*, 2021, **31**, 2006915.
- 18 C. Majidi and R. J. Wood, *Appl. Phys. Lett.*, 2010, **97**, 164104.
- 19 U.-C. Jeong, J.-H. Yoon, I.-H. Yang, J.-E. Jeong, J.-S. Kim, K.-H. Chung and J.-E. Oh, *Smart Mater. Struct.*, 2013, **22**, 115007.
- 20 J.-S. Oh, Y.-M. Han, S.-R. Lee and S.-B. Choi, *Smart Mater. Struct.*, 2013, **22**, 045004.
- 21 C. Cao and X. Zhao, *Appl. Phys. Lett.*, 2013, **103**, 041901.
- 22 A. Firouzeh, M. Salerno and J. Paik, *IEEE Trans. Rob.*, 2017, **33**, 765–777.
- 23 X. Huang, K. Kumar, M. K. Jawed, A. M. Nasab, Z. Ye, W. Shan and C. Majidi, *Sci. Rob.*, 2018, **3**, 7557.
- 24 X. Huang, K. Kumar, M. K. Jawed, A. Mohammadi Nasab, Z. Ye, W. Shan and C. Majidi, *Adv. Mater. Technol.*, 2019, 1800540.
- 25 T. L. Buckner, R. A. Bilodeau, S. Y. Kim and R. Kramer-Bottiglio, *Proc. Natl. Acad. Sci. U. S. A.*, 2020, **117**, 25360–25369.
- 26 M. J. Ford, C. P. Ambulo, T. A. Kent, E. J. Markvicka, C. Pan, J. Malen, T. H. Ware and C. Majidi, *Proc. Natl. Acad. Sci. U. S. A.*, 2019, **116**, 21438–21444.
- 27 P. Lv, X. Yang, H. K. Bisoyi, H. Zeng, X. Zhang, Y. Chen, P. Xue, S. Shi, A. Priimagi, L. Wang, W. Feng and Q. Li, *Mater. Horiz.*, 2021, **8**, 2475–2484.
- 28 Y. Chen, J. Yang, X. Zhang, Y. Feng, H. Zeng, L. Wang and W. Feng, *Mater. Horiz.*, 2021, **8**, 728–757.
- 29 M. Tatari, A. Mohammadi Nasab, K. T. Turner and W. Shan, *Adv. Mater. Interfaces*, 2018, **5**, 1800321.
- 30 A. M. Nasab, A. Sabzehzar, M. Tatari, C. Majidi and W. Shan, *Soft Rob.*, 2017, **4**, 411–420.
- 31 A. Mohammadi Nasab, P. Stampfli, S. Sharifi, A. Luo, K. T. Turner and W. Shan, *Adv. Mater. Interfaces*, 2022, 2102080.
- 32 S. Sharifi, A. Mohammadi Nasab, P.-E. Chen, Y. Liao, Y. Jiao and W. Shan, *Adv. Eng. Mater.*, 2022, 2101533.
- 33 A. Mohammadi Nasab, S. Sharifi, S. Chen, Y. Jiao and W. Shan, *Adv. Intell. Syst.*, 2020, 2000166.
- 34 Q. A. Acton, *Heavy Metals—Advances in Research and Application: 2013 Edition*, Scholarly Editions, 2013.
- 35 K. A. Shaikh and C. Liu, TRANSDUCERS 2007 – 2007 International Solid-State Sensors, Actuators and Microsystems Conference, 2007, pp. 2199–2202.
- 36 T. L. Buckner, M. C. Yuen, S. Y. Kim and R. Kramer-Bottiglio, *Adv. Funct. Mater.*, 2019, **29**, 1903368.
- 37 T. L. Buckner, M. C. Yuen and R. Kramer-Bottiglio, 3rd IEEE International Conference on Soft Robotics (RoboSoft), New Haven, 2020, pp. 259–265.
- 38 A. Mohammadi Nasab, T. Buckner, B. Yang and R. Kramer-Bottiglio, *Adv. Mater. Technol.*, 2021, 2100920.
- 39 A. Mann, T. Germann, M. Ruiter and P. Groche, *Mater. Des.*, 2020, **190**, 108580.

- 40 Z. Xia, D. B. Trigg, T. J. Montalbano and D. Rose, *J. Macromol. Sci., Part B: Phys.*, 2020, **59**, 390–398.
- 41 Y. Hao, J. Gao, Y. Lv and J. Liu, *Adv. Funct. Mater.*, 2022, **32**, 2201942.
- 42 C. S. O'Hern, L. E. Silbert, A. J. Liu and S. R. Nagel, *Phys. Rev. E: Stat., Nonlinear, Soft Matter Phys.*, 2003, **68**, 011306.
- 43 M. Wyart, S. R. Nagel and T. A. Witten, *Europhys. Lett.*, 2005, **72**, 486.
- 44 C. P. Goodrich, W. G. Ellenbroek and A. J. Liu, *Soft Matter*, 2013, **9**, 10993–10999.
- 45 D. Hexner, A. J. Liu and S. R. Nagel, *Phys. Rev. Lett.*, 2018, **121**, 115501.
- 46 N. Pashine, D. Hexner, A. J. Liu and S. R. Nagel, *Sci. Adv.*, 2019, **5**, eaax4215.
- 47 S. Dillavou, M. Stern, A. J. Liu and D. J. Durian, *Phys. Rev. Appl.*, 2022, **18**, 014040.
- 48 H. Yasuda, P. R. Buskohl, A. Gillman, T. D. Murphey, S. Stepney, R. A. Vaia and J. R. Raney, *Nature*, 2021, **598**, 39–48.
- 49 C. Kaspar, B. J. Ravoo, W. G. van der Wiel, S. V. Wegner and W. H. P. Pernice, *Nature*, 2021, **594**, 345–355.
- 50 T. Chen, M. Pauly and P. M. Reis, *Nature*, 2021, **589**, 386–390.
- 51 J. Ding and M. van Hecke, *J. Chem. Phys.*, 2022, **156**, 204902.
- 52 M. Bodaghi, R. Noroozi, A. Zolfagharian, M. Fotouhi and S. Norouzi, *Materials*, 2019, **12**, 1353.
- 53 R. Poon and J. B. Hopkins, *Adv. Eng. Mater.*, 2019, **21**, 1900802.
- 54 Q. Wu, C. Cui, T. Bertrand, M. D. Shattuck and C. S. O'Hern, *Phys. Rev. E*, 2019, **99**, 062901.
- 55 A. Parsa, D. Wang, C. S. O'Hern, M. D. Shattuck, R. Kramer-Bottiglio and J. Bongard, *Applications of Evolutionary Computation*, Cham, 2022, pp. 93–109.